This work was supported by NSF grant EAR-0510182 and by NWO grant 825.05.003

Healing of simulated fault gouges aided by pressure solution: results from rock analogue experiments

A.R. Niemeijer[1], Elsworth, D. [2] and Marone, C.J.[3]

[1] corresponding author, Pennsylvania State University, Energy Institute, Department of Geosciences, Department of Energy and Mineral Engineering, e-mail: arn3@psu.edu
[2] Department of Energy and Geo-Environmental Engineering
3 Department of Geosciences

PENN STATE ROCK AND SEDIMENT MECHANICS LABORATORY

1. Introduction

Fluids are important in the recovery of strength of faults between earthquakes. They exert a strong influence on the sliding behaviour of faults and fault gouges through both mechanical and chemical effects An increase in fluid pressure reduces the effective normal stress on a fault, effectively weakening the fault. On the other hand, pressure solution compaction and/or mineral precipitation strengthen the fault through an increase in packing density, an increase in contact area and/or an increase in the intrinsic strength of the sliding contacts. Despite it's importance, not much is known about the absolute rates of restrengthening (i.e. healing) under hydrothermal conditions. It is expected that the healing rate of a fault gouge will be strongly dependent on various parameters, such as the chemistry of the pore fluid, temperature and the "state" of the fault gouge (e.g the porosity, grain size distribution and the presence of shear bands). Moreover, it is known that phyllosilicates can have a strong influence on the actual rates of pressure solution compaction and they might act as inhibitors to contact strengthening. However, much of the previous work has been on pure quartz gouges under room temperature conditions where pressure solution is not active or to low strains. Moreover, previous studies have mostly neglected the possible effects of the state" of the fault gouge, i.e. the possible effects of accumulated strain.

2. Experimental methods

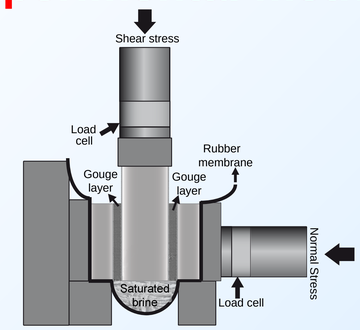

Figure 2.1. Schematic diagram of the experimental set-up

* Salt, ground and sieved to obtain grain size fraction of 106-212 μm. Industrial muscovite, used as received (d_{av}=13 μm).

* Gouge area of 5 X 5 cm^2 and initial gouge thickness of ~0.5 cm. Samples submerged in saturated brine.

* Initial run-in phase (10 mm displacement) at 5 μm/s and 10 MPa normal stress to reduce grain size reduction during the slide-hold-slide phase.

* Slide-hold-slide phase at 5 μm/s for slide distances of 2.5 mm and hold periods of 30, 100, 300, 1000, 3000 and 10000 seconds. A reverse slide-hold-slide scheme (10000, 3000, 1000, 300, 100 and 30 seconds) was also tested.

* A dry control experiment was run under controlled humidity.

3. Theoretical considerations

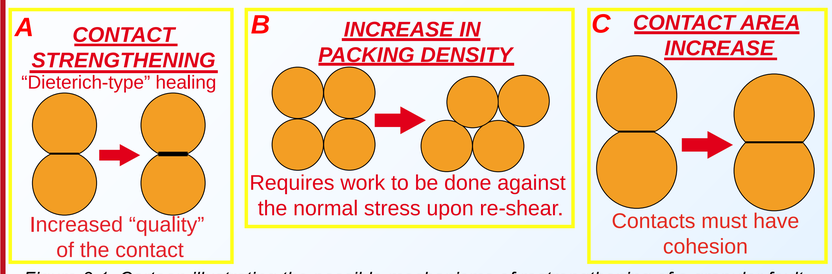

Figure 3.1. Cartoon illustrating the possible mechanisms of restrengthening of a granular fault gouge under conditions where pressure solution is active

The combined energy and entropy balance for a representative volume of fault rock during deformation can be written as:

$$\tau\dot{\gamma}+\sigma_n\dot{\varepsilon} = \dot{f}+\dot{\Delta}+\dot{A}_{gb}\gamma_{gb}+\dot{A}_{sl}\gamma_{sl}$$

Dividing by the strain rate, $\dot{\gamma}$, the measured shear stress can be written:

$$\tau = \tau_x - d\varepsilon/d\gamma\cdot\sigma_n$$

where $d\varepsilon/d\gamma$ represents an instantaneous dilatancy angle $tan\psi = d\varepsilon/d\gamma$ analogous to that familiar in soil mechanics and where

$$\tau_x = \frac{df}{d\gamma}+\frac{d\Delta}{d\gamma}+\frac{dA_{gb}}{d\gamma}\gamma_{gb}+\frac{dA_{sl}}{d\gamma}\gamma_{sl}$$

Table 3.1. Explanation of parameters. All parameters per unit volume of gouge.

Parameter	Explanation
τ	shear stress
$\dot{\gamma}$	shear strain rate
σ_n	normal stress
$\dot{\varepsilon}$	normal strain rate
$\dot{f}$	rate of change of Helmholtz free energy
$\dot{\Delta}$	energy dissipation rate by all irreversible processes
$\dot{A}_{gb}$	rate of change of grain boundary surface area
γ_{gb}	grain boundary surface energy
$\dot{A}_{sl}$	rate of change of solid-liquid interfacial area
γ_{sl}	solid-liquid interfacial energy
$d\varepsilon/d\gamma$	dilational work (≈ $tan\psi$)
ψ	dilatancy angle

4.1. Results: Mechanical data

Table 3.1. List of experiments performed and corresponding experimental conditions.

Sample ID	Composition wt% salt-muscovite	Pore fluid	Normal Stress MPa	Velocity μm/s	SHS periods seconds	Total strain	Final Porosity %
p1383	100 - 0	room-dry	5-10	5	30 - 100 - 300 - 1000 - 3000 - 10000	11.37	21.0
p1384	100 - 0	saturated brine	5-10	5	30 - 100 - 300 - 1000 - 3000 - 10000	11.51	6.6
p1385	80 - 20	saturated brine	5-10	5	30 - 100 - 300 - 1000 - 3000 - 10000	12.71	3.7
p1413	100 - 0	humidity < 6%	5-10	5	30 - 100 - 300 - 1000 - 3000 - 10000	10.25	18.2
p1414	100 - 0	saturated brine	5-10	5	10000 - 3000 - 1000 - 300 - 100 - 30	11.66	14.7
p1415	80 - 20	saturated brine	5-10	5	10000 - 3000 - 1000 - 300 - 100 - 30	12.38	14.2

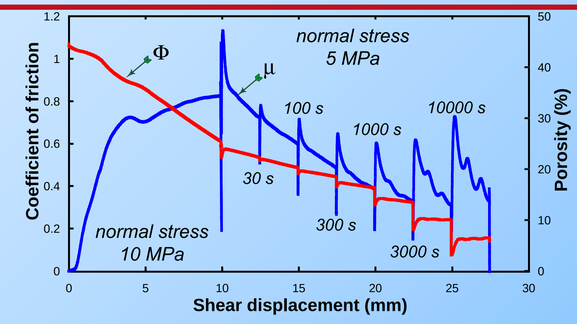

Figure 4.1. Typical stress-displacement curve for sample p1384 (salt brine-saturated). Also shown is the evolution of porosity.

4.2. Microstructures

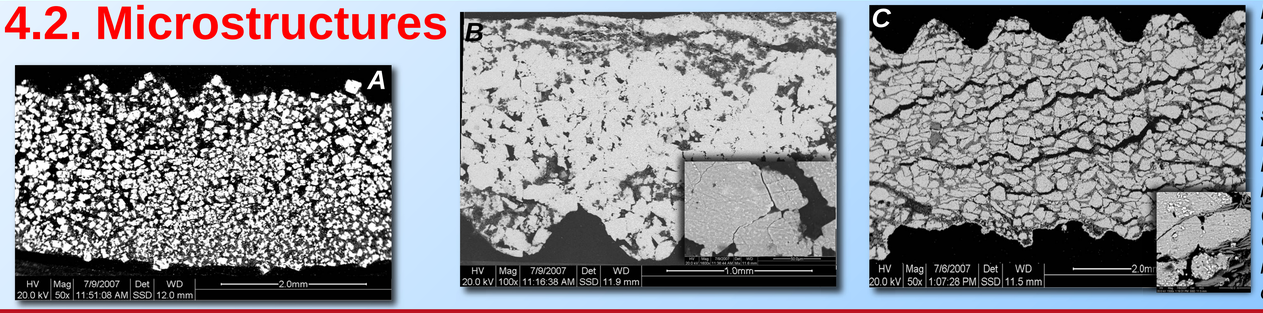

Figure 4.2. SEM BSE images of the observed microstructures. Shear sense is sinistral.
A. Sample p1413 (salt, controlled humidity). High porosity, porous regions at ~25º and grain size reduced compared to the starting fraction.
B. Sample p1384 (salt, brine-saturated). Dense gouge, highly cemented grain contacts, numerous grain-to-grain indentations.
C. Sample p1385 (salt + 20 wt% muscovite). Opened fractures in the Riedel orientation, numerous open muscovite-filled contacts, other contacts appear cemented.

4.3. Results: Healing data

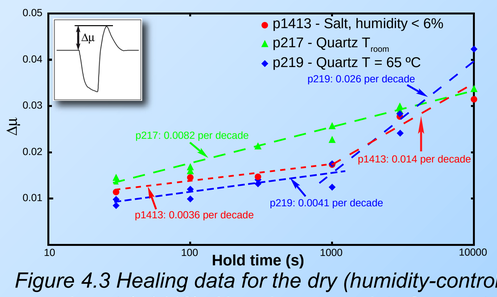

Figure 4.3 Healing data for the dry (humidity-controlled) experiment (p1413). Also shown are data for quartz (Yasuhara et al JGR 2005).

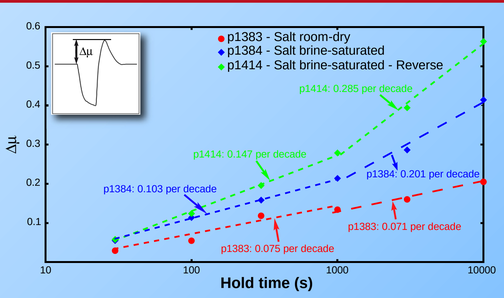

Figure 4.4. Healing data for all pure salt experiments. Note the break in slope, indicating a switch in dominant healing mechanism (e.g. activation of mechanism C at hold times of 1000 seconds).

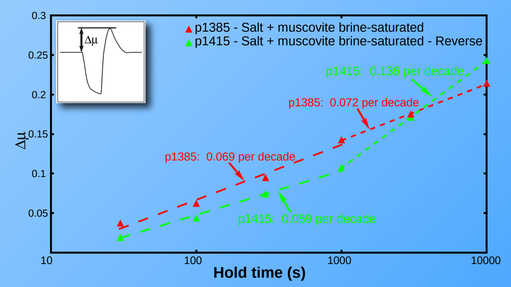

Figure 4.5. Healing data for all salt-muscovite experiments. Note again the break in slopes (especially in the reverse case) and the lower values of healing rates compared to pure salt.

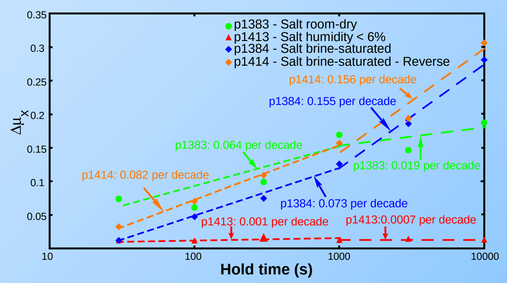

Figure 4.6. Healing data corrected for dilatational work for all salt samples. Dilatational work accounts for up to 80%. For deifinition of dmx, see theory. Note the break in slopes. Healing mechanism A (see Figure 3.1) is dominant at hold times <1000 seconds and C at longer hold times.

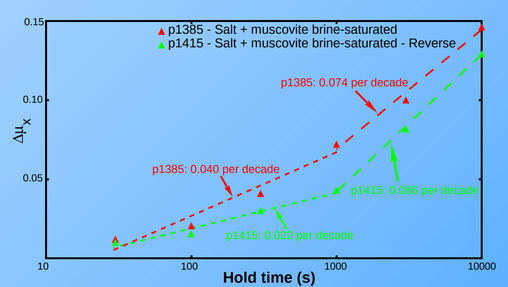

Figure 4.7. Healing data corrected for dilatational work for all salt-muscovite samples. Dilatational work accounts for up to 80%. Note the break in slopes.

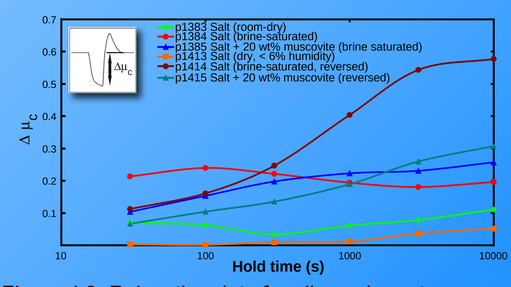

Figure 4.8. Relaxation data for all expeirments. Note the absence of relaxation in the dry case. Stress relaxation is dependent on the initial porosity at the start of the hold. In the reverse case, contacts are small initially (high porosity), leading to larger relaxation than in the forward case.

5. Conclusions

1. ***Healing in our simulated fault gouges is due to the operation of fluid-assisted processes (e.g. pressure solution).***
2. ***Up to 80% of the observed healing can be explained by consideration of dilatational work against the normal stress.***
3. ***A shift in healing rates is observed around hold times of ~1000 seconds and is probably related to the activation of a long term healing mechanism (pressure solution compaction).***
4. ***The presence of muscovite slows down healing by a factor of two. This could be due to the lower porosity sustained during shearing and/or inhibition of contact strengthening.***
5. ***Reversal of the slide-hold-slide scheme results in higher healing rates, presumably because of the higher initial porosities in the reversed experiments.***

Therefore, in order to reliably extrapolate laboratory healing rates to nature, some knowledge of the "state" (porosity, grain size, presence of foliation) of the fault gouge is required.

Future work will address the issue of permeability evolution in slide-hold-slide experiments.